RSC Advances

PAPER

View Article Online
View Journal | View Issue

Cite this: RSC Adv., 2017, 7, 5888

Highly conductive PEDOT:PSS treated by sodium dodecyl sulfate for stretchable fabric heaters†

C. Yeon,[ab] G. Kim,[ab] J. W. Lim[ab] and S. J. Yun*[ab]

In this study, the conductivity of poly(3,4-ethylenedioxythiophene):poly(4-styrenesulfonate) (PEDOT:PSS) was greatly enhanced by using sodium dodecyl sulfate (SDS) without damaging the fabric substrates. We suggest that blending and dipping methods using SDS which is compatible with natural and synthetic fabrics dramatically increase the conductivity of PEDOT:PSS to as high as 1335 S cm^{-1}. Additionally, a highly stretchable fabric heater with high conductivity was successfully fabricated using SDS-modified PEDOT:PSS. The fabric heaters exhibited reversible electrical behaviour with cyclic loading of a tensile strain even larger than 80%. The increase in resistance with the tensile strain was significantly smaller than the calculated value for a rigid substrate because the fabrics with a weave structure exhibited interfibrillar contact effects with strain. For example, the resistance was increased by a factor of only 2.62 with 80% strain. The Joule heating behaviours of the fabric heaters were demonstrated at several different applied voltages and ambient temperatures, and the heat capacity and convective heat transfer coefficient were 2 J K^{-1} and 30 W m^{-2} K^{-1}, respectively. The results demonstrated that the method suggested in this work is not only efficient for greatly improving the conductivity but also simple and cost-effective for fabricating highly conductive and stretchable fabrics with various e-textile applications.

Received 5th October 2016
Accepted 20th October 2016

DOI: 10.1039/c6ra24749k

www.rsc.org/advances

1. Introduction

Wearable heaters have recently attracted great interest as the demand for wearable and stretchable devices has grown.[1–7] Wearable heaters must be light-weight, comfortable to wear, and have the feel of a fabric.[8,9] However, conventional heating materials based on metal or metal wires have limitations, such as heaviness, inconvenience, and different textural properties between the heating material and fabric. To address these problems, many researchers have explored alternatives to metals, such as conducting polymers,[10–12] graphite,[13,14] graphene,[15] and carbon nanotubes.[16–19] Among these materials, conducting polymers are light-weight, processable, and flexible.[20] Since fabrics such as cotton and synthetic fabrics are not conductive, conducting materials must be loaded into the fabric; the simplest method for loading of fabrics is dipping the fabric into a solution containing the conductive polymer because fabrics can be well impregnated with aqueous solutions.[21] Poly(3,4-ethylenedioxythiophene):poly(4-styrenesulfonate) (PEDOT:PSS) is one of the most successfully commercialised conductive polymers owing to its high mechanical flexibility and excellent thermal stability.[22] However, the electrical conductivity of pristine PEDOT:PSS is less than 1 S cm^{-1}, which is too low to be utilised in heaters. High conductivity is a crucial factor affecting the conversion of electrical energy into thermal energy.

The conductivity of PEDOT:PSS has been reported to be increased by the addition of dielectric organic solvents, such as dimethyl sulfoxide (DMSO),[23] or by post-treatment with a strong acid.[24] However, the use of DMSO may irritate human skin, and fabrics are vulnerable to acid, preventing the use of post-treatment with a strong acid. Therefore, to improve the performance of PEDOT:PSS for application in the development of wearable heaters, it will be necessary to increase the conductivity of PEDOT:PSS without causing damage to the fabric.

Sodium dodecyl sulfate (SDS), one of the ionic surfactants that have been generally used in detergents for laundry, is effective for increasing the conductivity of PEDOT:PSS. It was reported that the conductivity of PEDOT:PSS film can be increased to 80 S cm^{-1} by adding SDS into PEDOT:PSS aqueous solution (hereafter, simply denoted by blending method).[25] However, previous study on the effect of anionic surfactants in PEDOT:PSS have not been studied in detail for achieving high conductivity.

In this study, we report the most effective and simple process using SDS for fabrication of highly conductive PEDOT:PSS, and SDS-modified PEDOT:PSS was evaluated as a conductive material in fabric heaters. The Joule heating properties of the stretchable fabric heater was also described.

[a]ICT Materials & Components & Research Laboratory, Electronics and Telecommunications Research Institute, 218 Gajeongno, Yuseong-gu, Daejeon 305-700, Korea. E-mail: sjyun@etri.re.kr

[b]Department of Advanced Device Engineering, University of Science and Technology, 217 Gajeongno, Yuseong-gu, Daejeon 305-350, Korea

† Electronic supplementary information (ESI) available. See DOI: 10.1039/c6ra24749k

2. Experimental section

2.1 Fabrications of PEDOT:PSS films and fabric heaters

PEDOT:PSS (Clevios PH1000) and the ionic agents were purchased from Heraeus and Sigma-Aldrich, respectively. Ionic agents with various functional groups, such as sulfate (SDS, lithium dodecyl sulfate [LDS]), sulfonate (sodium dodecylbenzene sulfonate [SDBS]), phosphate (sodium dodecyl phosphate [SDP]), cholate (sodium deoxycholate [SDC], sodium taurodeoxycholate [STDC], sodium cholate hydrate [SCH]), and ammonium (cetyltrimethylammonium bromide [CTAB]) were evaluated to determine which ionic agent was the most effective for increasing the conductivity of PEDOT:PSS. SDS was chosen for fabricating PEDOT:PSS-fabrics. Blending was carried out by adding SDS (0–40 mM) into the PEDOT:PSS solution, stirring at 80 °C for 1 h, and filtering of the solution using a 5 μm poly(1,1,2,2-tetrafluoroethylene) filter. For the dipping method, the fabrics were impregnated with PEDOT:PSS solution, dried for 30 min at 110 °C, and dipped in SDS solution. The concentration of SDS in dipping solution ranged from 0 to 400 mM. The novel method introduced in this work was to conduct the dipping process for a sample coated with SDS-blended PEDOT:PSS. For all of the methods, the samples were dried at 110 °C as the final step of fabrication.

2.2 Characterization of PEDOT:PSS films and fabric heaters

Prior to fabricating PEDOT:PSS-fabrics, the solution was spin-coated on glass pretreated by UV–ozone to characterise the PEDOT:PSS films. We measured the sheet resistance and film thickness of the PEDOT:PSS films using the four-point probe system and a surface profiler (Alpha-Step IQ, KLA-Tencor), respectively. An ultraviolet-visible (UV-Vis)/near-infrared (NIR) spectrophotometer (LAMBDA 750; Perkin-Elmer) was used to measure the transmittance and absorbance of the PEDOT:PSS films. The influence of the ionic agent on the chemical bonding states of the films was investigated using confocal Raman microscopy (ARAMIS, Horiba Jobin Yvon) with 785 nm laser and FT-IR spectrophotometer (Nicolet iS50, Thermo Fisher). To collect the FT-IR spectra, the solution was spin-coated on a KBr window (PIKE Tech.) and then annealed at 120 °C. We observed surface states of the films by optical microscopy (STM6-F10-2; Olympus). Topographic and phase images of the films were obtained using AFM (XE-100, PARK System). We performed stability tests with strain under constant environmental conditions (relative humidity and temperature: 40% and 22.5 °C, respectively).

The Joule heating behaviours of fabric heaters were investigated under constant voltages (6, 9, and 12 V) supplied by a DC power source (RDP-305; SMART). We measured the temperatures of the heaters using a digital thermometer (UT320; UNI-T) and observed their IR images using a thermal camera (Therm-App TH, Therm-App). The resistances of the fabric heaters with or without strain were obtained from *I–V* characteristic curves of the samples using a source meter (4200-SCS; Keithley). The joule heating experiment was carried out at an ambient temperature of 26 °C. The experiment at 4 °C was also carried out in a refrigerator to show the heating behaviour in a cold environment.

3. Results and discussion

Surfactants with various functional groups, including sulfate, sulfonate, phosphate, cholate, and ammonium, were evaluated to determine which surfactant was the most effective for increasing the conductivity of PEDOT:PSS. Among the surfactants tested in this study, the surfactants with sulfate and sulfonate groups caused dramatic increases in conductivity (ESI Fig. S1†). However, the addition of surfactants with phosphate, cholate, and ammonium functional groups did not result in any considerable increase in conductivity and caused a noticeable aggregation in the solution. Based on this screening, we chose SDS, which consisted of a 12-carbon tail attached to a sulfate group.

We suggested two methods for applying SDS to PEDOT:PSS for applications involving fabrics: the blending method, in which fabrics are impregnated with a PEDOT:PSS aqueous solution blended with SDS; and the dipping method, in which fabrics are dipped in an aqueous solution containing PEDOT:PSS and SDS. In order to develop the most effective process for achieving high electrical conductivity and mechanical stability for applications as wearable heaters, the effects of SDS blending and dipping methods were evaluated by varying the SDS concentration.

A glass substrate was used for the electrical characterization of PEDOT:PSS films formed by blending and dipping methods. The conductivity and thickness of the films formed by the blending method (denoted as B-PEDOT:PSS films) are plotted with respect to the SDS concentration in the blended solution in Fig. 1a. The conductivity of the PEDOT:PSS film logarithmically increased as the SDS concentration was increased from 0 to 40 mM, and the highest conductivity of 465 S cm^{-1} was achieved at 40 mM SDS. The film thickness also increased gradually from 80 to 110 nm with as the SDS concentration increased. A non-uniform film was obtained at concentrations above 40 mM, owing to aggregation during spin-coating. The conductivity and thickness of the films formed by the dipping method (denoted as D-PEDOT:PSS films) are shown in Fig. 1b. The conductivity was significantly increased from 0.5 to 1008 S cm^{-1} with increasing concentrations of SDS solution from 0 to 400 mM. Additionally, the film thickness decreased from 80 to 30 nm with increasing concentrations of SDS aqueous solution, similar to the behaviour of PEDOT:PSS films treated with a strong acid, such as H_2SO_4, HNO_3, or HCl.[26,27] Thus, these results suggested that the mechanism of conductivity enhancement in PEDOT:PSS for blending and dipping methods is quite different.

The stability test was performed under constant conditions (relative humidity and temperature were 40% and 22.5 °C, respectively) for 7 days. As shown in Fig. 1c, the conductivities of B-PEDOT:PSS and D-PEDOT:PSS films remained almost unchanged, while the pristine PEDOT:PSS film underwent severe degradation. The normalised conductivity (σ/σ_0) with respect to time is shown in the inset in Fig. 1c, where the value

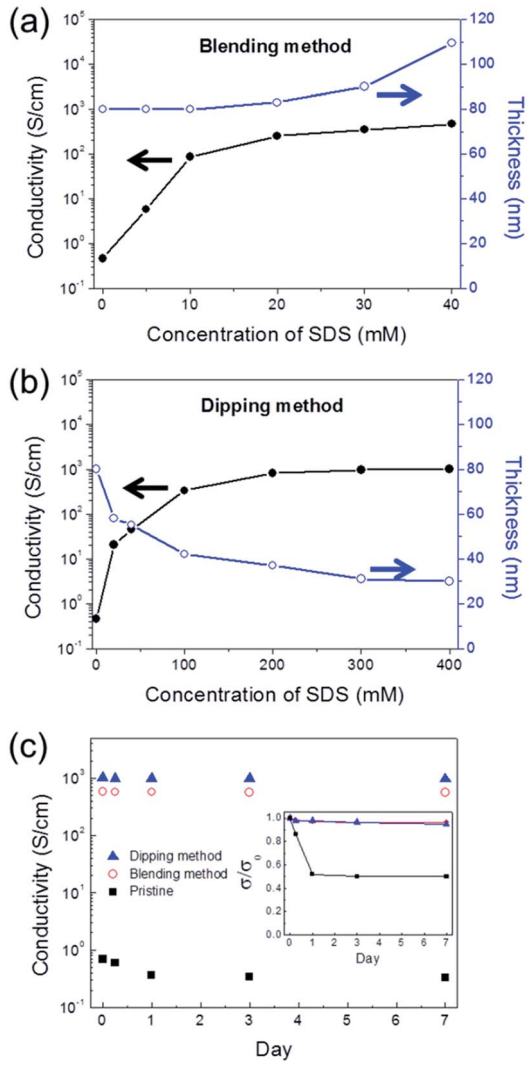

Fig. 1 Average conductivities and thickness of (a) B-PEDOT:PSS and (b) D-PEDOT:PSS. (c) Electrical stability tests of pristine-, B-, and D-PEDOT:PSS under constant conditions (relative humidity and temperature: 40% and 22.5 °C, respectively) for 7 days. The inset shows the normalised conductivity with respect to time.

of σ/σ_0 at a time represents the ratio of the initial conductivity (σ_0) and the conductivity measured after the time (σ). The σ/σ_0 of the pristine PEDOT:PSS film decreased to 0.5 within 1 day. In contrast, the σ/σ_0 values of B-PEDOT:PSS and D-PEDOT:PSS films were 0.96 and 0.95, respectively, after 7 days.

To investigate the mechanism of conductivity enhancement through the blending and dipping methods, the analysis of chemical bonding states of PEDOT:PSS films was carried out using absorption spectroscopy. The absorption spectra of the PEDOT:PSS films formed by SDS blending (40 mM) and SDS dipping (40, 100, 200, and 400 mM) are shown in Fig. 2a. Notably, the D-PEDOT:PSS films showed significant decreases in absorbance at 5.5 eV, where a strong absorption band originated from the aromatic rings of PSS.[28] This result demonstrated that insulating PSS in the film was selectively removed. A small increase in absorbance in the region from 1 to 2 eV was also observed, indicating the generation of polaronic states in the bandgap due to enhancement of the interchain interaction between the conducting domains.[29] In contrast, for the B-PEDOT:PSS film, absorbance in the UV light region increased due to absorption by SDS, with no increase in absorbance in the region from 1 to 2 eV (ESI Fig. S2†).

Raman spectroscopic analysis was also carried out to investigate conformational changes in the pristine and SDS-modified PEDOT:PSS films. As shown in Fig. 2b, the Raman spectra showed two intensive peaks, which could be attributed as follows: 1438 cm^{-1} to C_α–C_β symmetric stretching vibrations, 1373 cm^{-1} to C_β–C_β deformations.[30] The Raman spectrum of the B-PEDOT:PSS film showed an 8 cm^{-1}-shifted C_α–C_β symmetric stretching vibrational peak to a higher energy compared with that of pristine PEDOT:PSS. The degree of blue shift of the C_α–C_β symmetric stretching peak gradually increased with the concentration of SDS (ESI Fig. S3†). These results suggested that the SDS introduced into PEDOT:PSS solution can replace PSS as the counter-anions to PEDOT chain resulting in conformational change from benzoid (coiled) to quinoid (linear) structure.[25,31] Contrary to pristine- and B-PEDOT:PSS films, the C_α–C_β symmetric stretching peak of the D-PEDOT:PSS film was red-shifted. Although this red-shift implied that the conformation of PEDOT:PSS was changed from quinoid to benzoid structure, conductivity of D-PEDOT:PSS dramatically increased because the PEDOT oxidation state changes from bipolaron to polaron by the PSS removal as supported by the increase of polaronic states in absorption spectra of Fig. 2a.

The conformational change of PEDOT:PSS could also affect the bonding energy between constituent atoms in PEDOT:PSS.[32] Thus, FT-IR analysis was performed to investigate the change of bonding energy. As shown in Fig. 2c, the FT-IR spectrum of the pristine PEDOT:PSS showed peaks at 1209, 1143, and 1089 cm^{-1} which are originated from to C–O–C bond stretching in the ethylene dioxy group.[33,34] The C–S bond stretching peaks in the thiophene ring were observed at 977, 827, and 690 cm^{-1}.[33,34] The peaks assigned at 1544 and 1342 cm^{-1} correspond to C=C and C–C bonds, respectively.[33,34] These peaks in the FT-IR spectrum of D-PEDOT:PSS shifted to higher bonding energies, while the FT-IR spectrum of B-PEDOT:PSS was similar to that of pristine-PEDOT:PSS. In particular, the peak of 1342 cm^{-1} corresponding to the C–C bond shifted to 1432 cm^{-1}, which means that the C–C bonding energy increased due to the PSS removal by SDS dipping.

Based on the results, schematic conformations of the pristine-, B-, and D-PEDOT:PSS were illustrated in Fig. 2d. The SDS blending method induces the conformational change from coiled to linear structure by introducing SDS molecules and the SDS dipping method selectively removes PSS domains to increase the interchain interactions between PEDOT-rich cores.

Distinct changes in the surface morphologies of B- and D-PEDOT:PSS films were observed by atomic force microscopy (AFM). The AFM images of topography in Fig. 3a, c and e demonstrate that the rms roughness (R_q) values of the pristine- and B-PEDOT:PSS films were 1.3 and 1.4 nm, respectively, and the R_q of D-PEDOT:PSS films increased to 2.2 nm. Fig. 3b, d and f show phase images in which the positively charged (bright) and negatively charged (dark) phases corresponded to

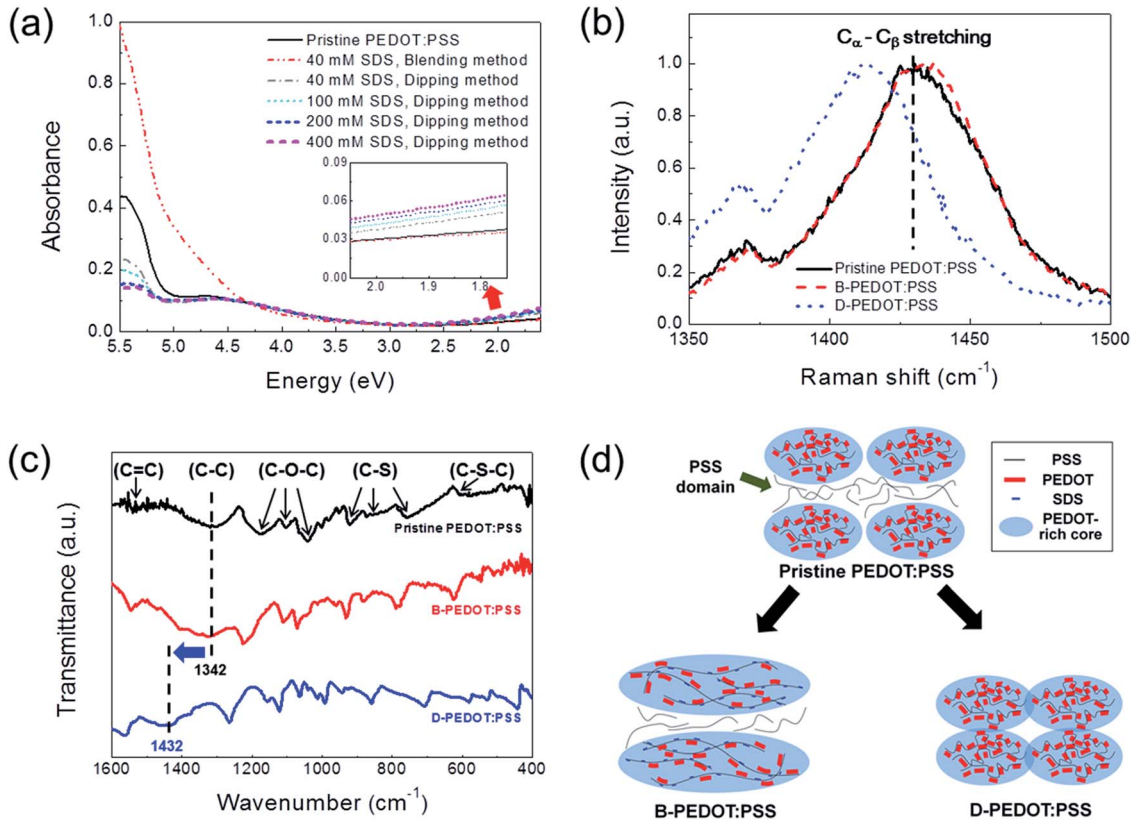

Fig. 2 (a) UV-Vis/NIR absorption spectra of the pristine-, B-, and D-PEDOT:PSS films. The inset of the UV-Vis/NIR absorption spectra shows the increase in the absorption band in the region of 1.7 to 2 eV. (b) Normalised Raman and (c) FT-IR spectra of the pristine-, B- (40 mM), and D-PEDOT:PSS (400 mM) films. (d) Schematic conformations of the pristine-, B-, and D-PEDOT:PSS films.

PEDOT-rich and PSS-rich grains, respectively.[35] These results clearly supported that the SDS dipping method induced selective removal of PSS domains. In contrast, the phase image of B-PEDOT:PSS (Fig. 3d) was similar to the image of pristine-PEDOT:PSS (Fig. 3b), indicating that the conductivity enhancement conferred by the SDS blending method was caused not by PSS removal but by conformational change of PEDOT chains.

Next, we found that application of the blending method followed by the dipping method could further increase the conductivity. As shown in Fig. 4a, the highest conductivity of 1335 S cm^{-1} could be achieved by using both the blending and dipping methods. The same trend was obtained in the case of the fabric impregnated with PEDOT:PSS (ESI Fig. S4†).

Fabrics can be easily impregnated with aqueous PEDOT:PSS solution as long as the fabrics can be wetted by water. In this study, 100% polyurethane (denoted as polyurethane) and 98% cotton/2% polyurethane (denoted as cotton), which exhibited high stretchability, were used for the fabrication of conductive and stretchable fabric (ESI Fig. S5†). Hereafter, the fabrics impregnated in SDS-blended PEDOT:PSS solution followed by dipping SDS aqueous solution are denoted as BD-PEDOT:PSS-fabrics. As shown in Fig. 4b, the sheet resistances (R_S) for BD-PEDOT:PSS-cotton and -polyurethane were 24 and 48 Ω $\square^{-1}$, respectively. The results indicated that the R_S of the BD-PEDOT:PSS-cotton was lower than that of the BD-PEDOT:PSS-polyurethane because the amount (1.6 mg cm^{-2}) of PEDOT:PSS coated on the cotton was higher than that (0.7 mg cm^{-2}) coated on the polyurethane. Furthermore, the R_S value could be gradually decreased by increasing the number of coatings (ESI Fig. S6†). Depending on the porosity and hydrophilicity of fabrics, the R_S of BD-PEDOT:PSS-fabric could be further decreased, and the style of weave that could absorb large amounts of PEDOT:PSS was important for achieving a low R_S value.

In order to investigate the stretchability of the PEDOT:PSS-modified fabrics and to determine which fabric would be most valuable for conferring conductivity, the resistance was measured under tensile strain (ε). The initial resistance of a sample before loading any strain, R_0, is described by eqn (1),

$$R_0 = \frac{1}{\sigma}\frac{l}{wh} \quad (1)$$

where σ, l, w, and h are the conductivity, length, width, and height of the sample with no strain, respectively. Because the dimensions of the sample change with strain, the resistance with strain, R_{St}, can be expressed by eqn (2),[37]

$$R_{St} = \frac{1}{\sigma}\frac{l\left(1+\varepsilon'\right)}{w\left(1-\nu_s\varepsilon'\right)h\left(1-\nu_f\varepsilon'\right)} \quad (2)$$

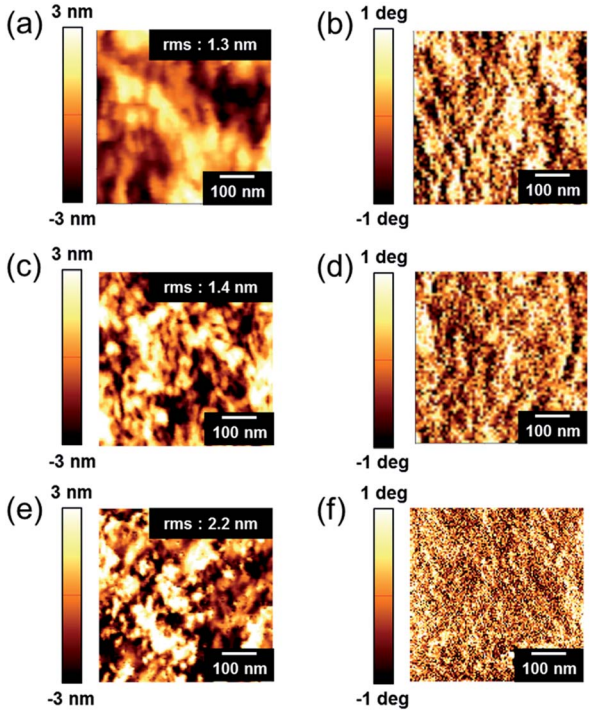

Fig. 3 AFM images of the pristine- [(a) and (b)], B- [(c) and (d)], and D-PEDOT:PSS films [(e) and (f)]. The left (a, c, e) and right (b, d, f) images are photographic and phase images, respectively. The concentrations of SDS used for blending and dipping methods were 40 and 100 mM, respectively. All images were obtained for an area of 250 nm × 250 nm.

where ν_s and ν_f are the Poisson's ratio of the substrate and film, respectively, and ε' is the fractional strain defined as $\varepsilon' = \varepsilon/100\%$. Then, the normalised resistance, R_{St}/R_0, can be simply expressed by eqn (3),

$$\frac{R_{St}}{R_0} = \frac{1+\varepsilon'}{(1-\nu_s\varepsilon')(1-\nu_f\varepsilon')} \quad (3)$$

The woven structure of the fabric related to the Poisson's ratio determines its structural and mechanical properties.[38] Thus, the ν_s values of cotton and polyurethane used as fabric substrates in this work were measured to be 0.48 and 0.2, respectively. The reported ν_f of PEDOT:PSS was 0.3532. As shown in Fig. 5a, we plotted R_{St}/R_0 with respect to ε for BD-PEDOT:PSS-cotton (solid line), where the resistances were directly measured from the current (I)–voltage (V) characteristic curves of the samples. The method of I–V measurement is described in detail in Fig. S7.† The R_{St}/R_0 values calculated using the ν_s and ν_f mentioned above are shown in Fig. 5a (dotted line). The measured R_{St}/R_0 values with $\varepsilon \leq 20\%$ were consistent with the calculated values, and the differences between them increased with ε when $\varepsilon > 20\%$. For example, at $\varepsilon = 80\%$, the measured R_{St}/R_0 of the BD-PEDOT:PSS-cotton was 2.62, while the calculated R_{St}/R_0 was 4.05. The significantly small increase in the real R_{St} with ε compared with the calculated value must be caused by the woven structure of the fabric. The stretching of the fabric improves the alignment and intercontact of the fibres, thereby reducing its resistance.[39,40] Hereafter, we call this effect the "interfibrillar contact effect".

Next, the cyclic ε-loading/unloading tests were performed for BD-PEDOT:PSS-cotton was also performed and the result was shown in Fig. 5b. The R_{St}/R_0 shows reversible behaviour with cyclic ε-loading/unloading. The inset in Fig. 5b shows the changes in R_{St}/R_0 during a cycle of ε-loading/unloading. The difference of R_{St}/R_0 between $\varepsilon = 0\%$ (blue arrow) and 20% (red arrow) was only 0.09. However, the difference gradually decreased with the strain, and finally showed reaching a negative value. For example, the difference was decreased from 0.09 to −0.20 when the strain increased from 20% to 80%. The results clearly indicated that the interfibrillar contact effect increased with ε due to the increase of in the interfibrillar contact area along with the axis of ε until the cotton was torn at $\varepsilon > 80\%$.

We also carried out I–V measurement and cyclic ε-loading/unloading tests for BD-PEDOT:PSS-polyurethane, which was stretchable even with an extreme strain greater than 150%. The

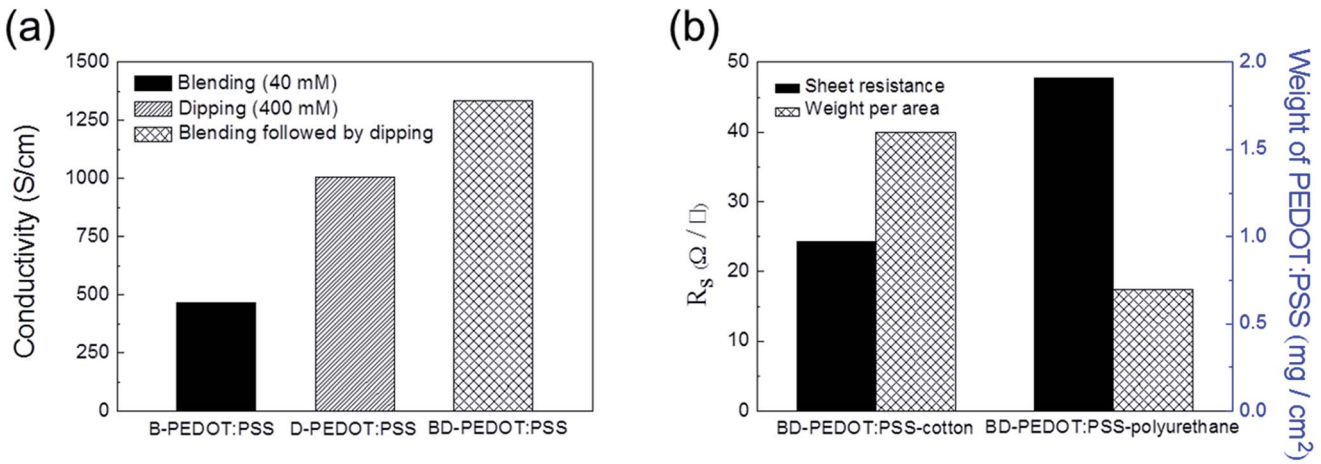

Fig. 4 (a) The highest conductivities of B-, D-, and BD-PEDOT:PSS films spin-coated on glass. (b) Sheet resistance (R_S) and weight of PEDOT:PSS of BD-PEDOT:PSS-cotton and polyurethane.

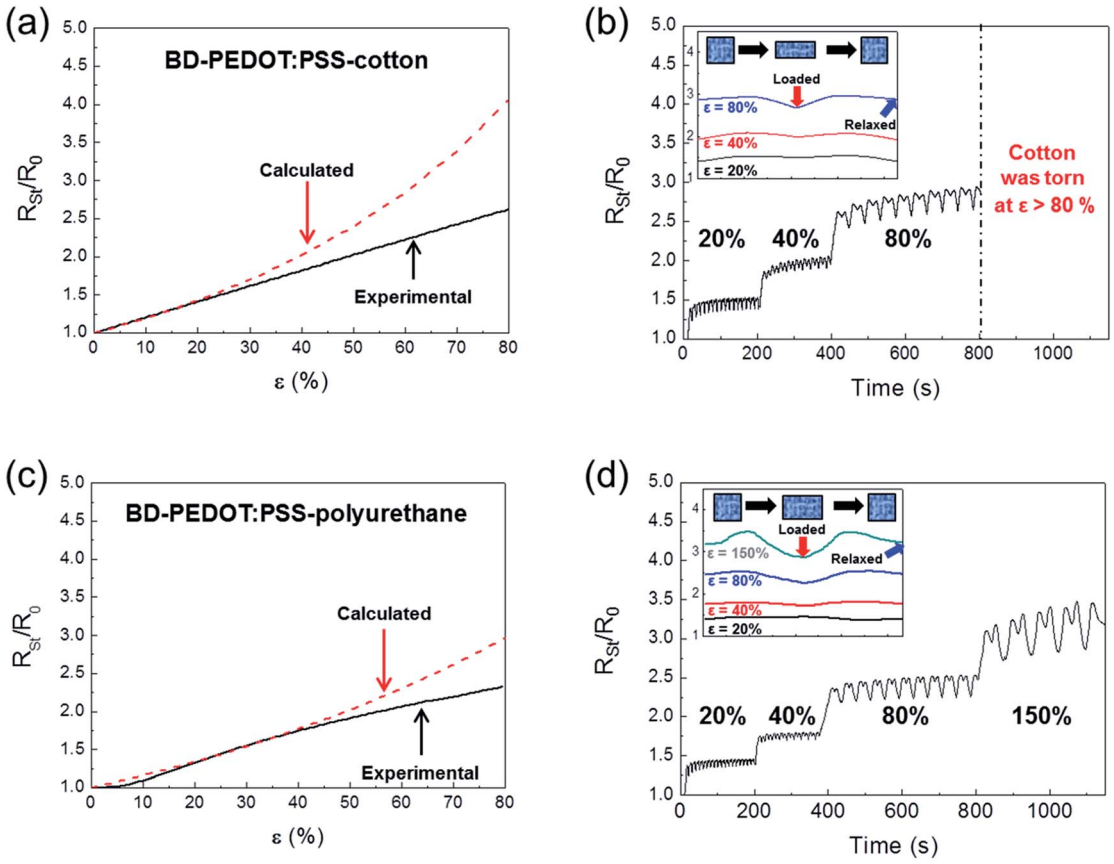

Fig. 5 Normalised resistance results of (a) BD-PEDOT:PSS-cotton and (c) BD-PEDOT:PSS-polyurethane with respect to tensile strain. The dotted and single curves correspond to the calculated and experimental data, respectively. Cyclic loading tests for (b) BD-PEDOT:PSS-cotton and (d) BD-PEDOT:PSS-polyurethane. The insets of (b) and (d) show changes in R_{St}/R_0 during a cycle of ε-loading.

calculated and experimental R_{St}/R_0 curves for BD-PEDOT:PSS-polyurethane are shown in Fig. 5c. The measured R_{St}/R_0 values with $\varepsilon = 40\%$ coincided with the calculated values, and the difference between them then increased with ε when $\varepsilon >$ 40%. The results of cyclic ε-loading/unloading tests for BD-PEDOT:PSS-polyurethane are shown in Fig. 5d. Interestingly, the R_{St}/R_0 values of BD-PEDOT:PSS-polyurethane were saturated after only a few cycles of ε-loading/unloading, even with an ε value as large as 80%, and the results consistently showed reproducible curves by ε-loading/unloading. The inset of Fig. 5d clearly demonstrates that the interfibrillar contact effect was still effective with $\varepsilon = 150\%$.

In this work, we introduce the term "critical interfibrillar contact strain (ε_{CIC})", above which the experimental R_{St}/R_0 values begin to deviate from the values calculated using Poisson's ratios; when $\varepsilon > \varepsilon_{CIC}$, $(R_{St}/R_0)_{exp} < (R_{St}/R_0)_{cal}$ for a positive interfibrillar contact effect. As shown in Fig. 5a and c, the ε_{CIC} of BD-PEDOT:PSS-polyurethane ($\nu_s = 0.2$) was 40%, while the ε_{CIC} of BD-PEDOT:PSS-cotton ($\nu_s = 0.48$) was 20%. These results implied that the value of ν_s was related to ε_{CIC} and that larger ν_s values resulted in smaller ε_{CIC} values. Moreover, higher ν_s values could more effectively facilitate increased interfibrillar contact effects during stretching.

As shown in Fig. 5b and d, the relaxed resistance, R'_0, even after one cycle of ε-loading/unloading, was larger than R_0, and R_{St}/R_0 was not recovered to the initial value of 1.0. This may be explained by the permanent deformation of the conducting films owing to cracking or peeling. To investigate the reason for this deformation, we used optical microscopy and scanning electron microscopy (SEM) before and after ε-loading for the BD-PEDOT:PSS-cotton, which was relatively weak against strain compared with BD-PEDOT:PSS-polyurethane. Fig. 6a shows optical and SEM images of the BD-PEDOT:PSS-cotton before and after ε-loading. These optical images showed that the BD-PEDOT:PSS-cotton (purple colour) was uniformly coated by PEDOT:PSS. The SEM image in Fig. 6b does not show any visible fractures after loading 40% of ε. However, the PEDOT:PSS films showed signs of peeling at $\varepsilon = 150\%$ (ESI Fig. S8†). In a previous study, a compressive force perpendicular to the stretching direction was exerted on the film during stretching, leading to the formation of cracks when the Poisson's ratio of the substrate was larger than that of the film,[36] and we observed cracks in SDS-modified PEDOT:PSS coated on polydimethylsiloxane, even after loading 40% of ε (ESI Fig. S9†). These results demonstrated that the woven structure significantly relieved stress from the compressive force; therefore, BD-PEDOT:PSS-fabric exhibited excellent stretchability while maintaining low resistance. This low resistance behaviour with a very large ε may be a noticeable advantage of conductive fabric applications compared with conventional plastic applications.

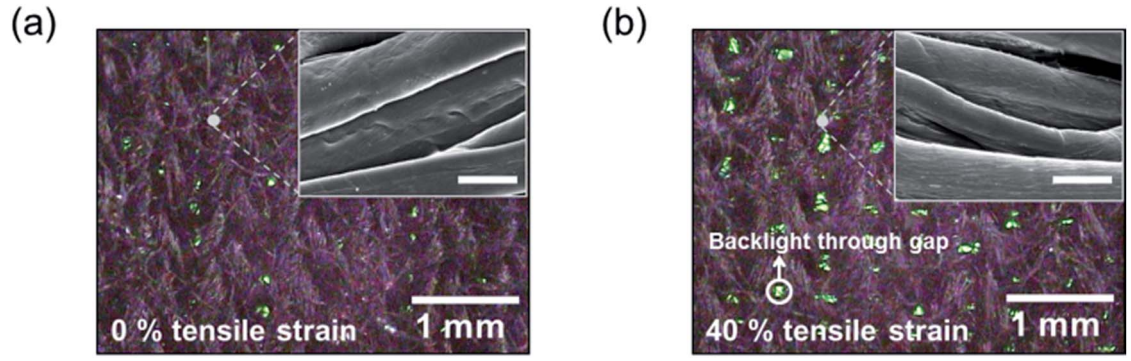

Fig. 6 Optical and SEM images of the BD-PEDOT:PSS-cotton before (a) and after (b) loading 40% tensile strain. The scale bar of the SEM image is 10 μm.

Using the BD-PEDOT:PSS-cotton, we fabricated a flexible heater to determine the applications of stretchable conducting fabrics and evaluated the Joule heating behaviours of this heater. Fig. 7a shows the temperature (T)–time (t) profiles for the BD-PEDOT:PSS-cotton, which had an R_S of 24 Ω $\square^{-1}$. When a bias voltage (6, 9, or 12 V) was applied, the temperature of the fabric heater increased and saturated to a certain temperature within 60 s. For example, the saturated temperature (T_{sat}) of BD-PEDOT:PSS-cotton was 99.6 °C when 12 V was applied. The heat capacity (C) and convective heat transfer coefficient (h) could be also obtained by comparing the experimental data with the T–t curve calculated using a power balance equation.[41]

In general, a power balance equation[41] between the input power and heat loss by convection (Q_{conv}) and radiation (Q_{rad}) can be described as shown in eqn (4),

$$\frac{V^2}{R} = Q_{conv} + Q_{rad} + C\frac{dT}{dt} \quad (4)$$

where V and R are the input voltage and resistance, respectively. Q_{conv} and Q_{rad} are expressed as shown in eqn (5) and (6),

$$Q_{conv} = hA(T - T_0) \quad (5)$$

$$Q_{rad} = e\sigma A(T^4 - T_0^4) \quad (6)$$

where A, T_0, e, and σ are the convective heat transfer coefficient, the surface area of the heater (10.8 cm^2), initial temperature, surface emissivity of the heater (0.98), and Stefan–Boltzmann constant (5.67 × 10^{-8} W m^2 K^{-4}), respectively. Because R increased with T, the temperature coefficient of resistance (α) was introduced, and α was 0.001 K^{-1} by measuring the current with respect to the temperature. The power balance equation (eqn (4)) can be expanded by using eqn (5) and (6), as expressed in eqn (7),

$$\frac{V^2}{R_0\left\{1 + \alpha(T - T_0)\right\}} = hA(T - T_0) + e\sigma A\left(T^4 - T_0^4\right) + C\frac{dT}{dt} \quad (7)$$

where R_0 is initial resistance. When the values of C and h were 2 J K^{-1} and 30 W m^{-2} K^{-1}, respectively, the calculated curve coincided quite well with the measured data of BD-PEDOT:PSS-cotton, as shown in Fig. 7a.

To evaluate the potential of stretchable PEDOT:PSS-fabric heaters, the Joule heating behaviours were investigated with different ε values. As shown in Fig. 7b, the value of T_{sat} decreased slightly from 99.6 to 97.7 °C at $\varepsilon = 10\%$. Additionally, the T_{sat} was 80.4 °C at $\varepsilon = 80\%$. The values of T_{sat} with respect to ε were plotted in Fig. S10.† As inferred from Fig. 5a, the experimental values of T_{sat} with $\varepsilon > 20\%$ were larger than the calculated values due to the interfibrillar effect. These results indicated that the BD-PEDOT:PSS-fabric was a promising material for application in highly stretchable heaters.

In practical applications, fabric heaters may be used in a cold environment. Therefore, the heating behaviours were also investigated in a low-temperature environment (4 °C) and compared with the heating behaviours at room temperature (26 °C). As shown in Fig. 7c, the T_{sat} of BD-PEDOT:PSS-cotton was 88.0 °C, while the value at room temperature was 99.6 °C. Furthermore, a longer time was needed to reach saturation at 4 °C than at 26 °C. This result could be explained by changes in h depending on environmental conditions (the speed of convection currents, *etc.*).[42]

We also obtained photographs and infrared images of a human hand wearing the fabric heater, as shown in Fig. 7d. In this experiment, the input voltage was as mild as 6 V to avoid the potential danger of burns. The maximum (T_{max}) and minimum temperatures (T_{min}) were 46.1 and 41.9 °C, respectively, before bending the finger, and 46.9 and 42.6 °C, respectively, after bending the finger. The results clearly show that BD-PEDOT:PSS-fabric can be adaptable even for the finger joint or elbow requiring very high stretchability ($\varepsilon > 100\%$).

As described above, because a few cycles are needed to reach a stable reversible behaviour, a cycle-aging process at a certain ε is essential for practical applications requiring consistent reproducible performance. Fig. 8 shows the $R_{St}/R_{0,sat'}$ values of BD-PEDOT:PSS-fabrics during a cycle of 80% ε-loading/unloading, where $R_{0,sat'}$ is the saturated resistance of a sample at $\varepsilon = 0\%$ after suffering from cycle-aging processing at $\varepsilon = 80\%$. The results showed that the differences between the maximum and minimum $R_{St}/R_{0,sat'}$ values for BD-PEDOT:PSS-cotton and

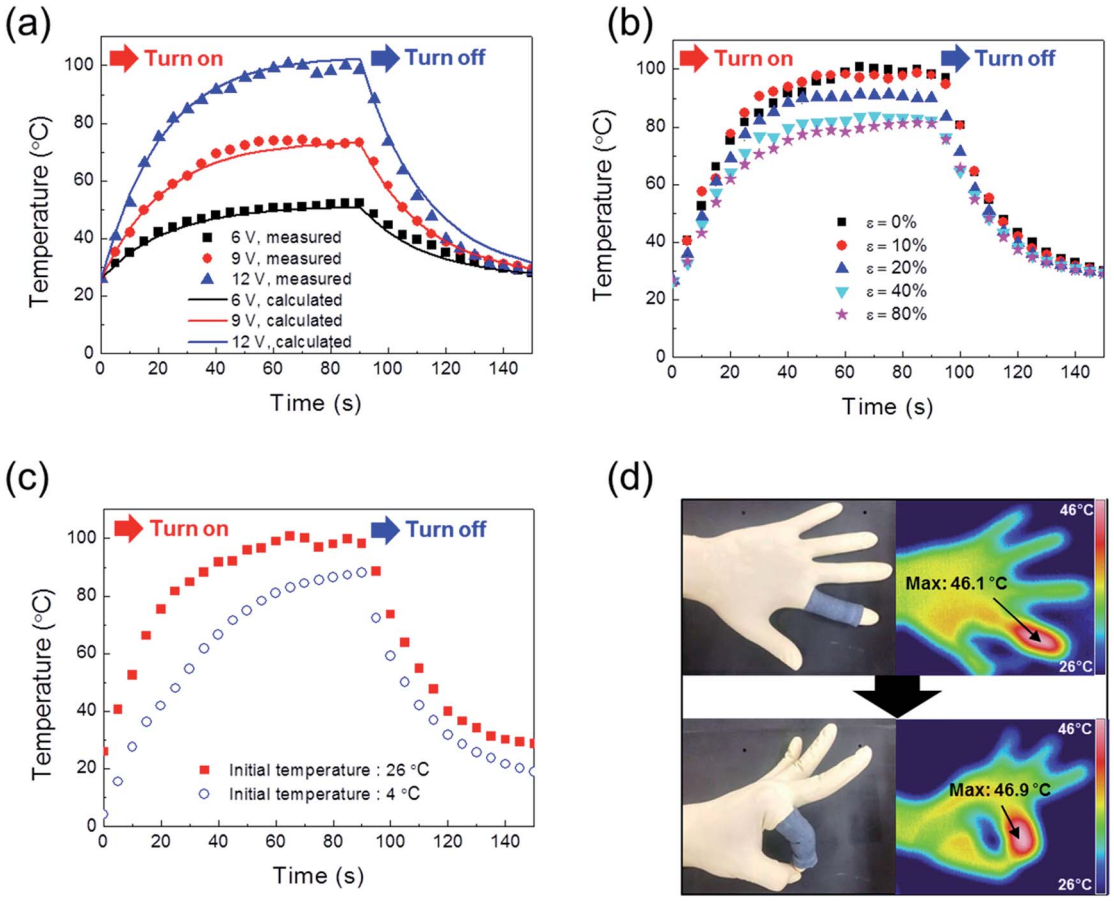

Fig. 7 (a) Temperature–time dependence curve with application of different bias voltages (6, 9, and 12 V). The solid lines are fitted curves calculated from a power balance equation between input power and heat loss. (b) Joule heating properties as a function of tensile strain at an applied voltage of 12 V. (c) Heating properties at an applied voltage of 12 V under different ambient temperatures (4 and 26 °C). (d) Photographs and IR images of the heaters before and after bending fingers. The applied bias voltage was 6 V.

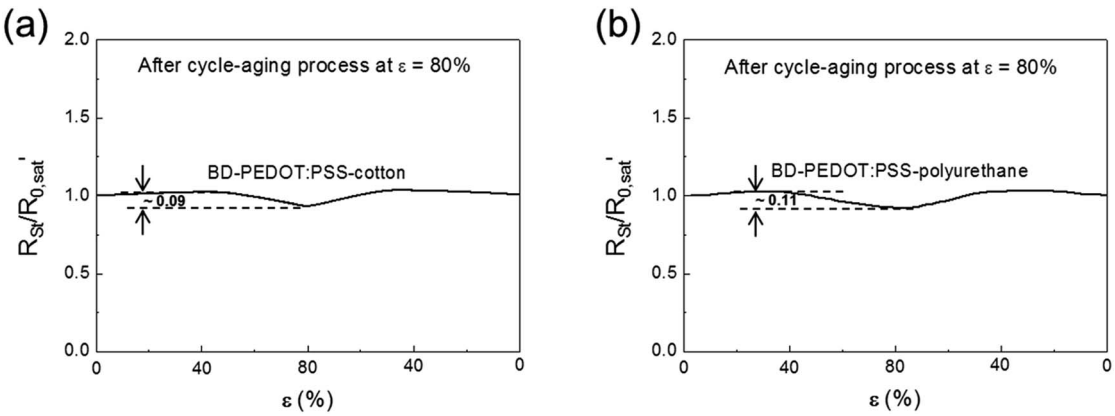

Fig. 8 The $R_{St}/R_{0,sat'}$ values of (a) BD-PEDOT:PSS-cotton and (b) BD-PEDOT:PSS-polyurethane during a cycle of 80% loading after performing the cycle-aging process at $\varepsilon = 80\%$.

polyurethane were 0.09 and 0.11, respectively; these values are so small that stretchable device performance would not be noticeably changed with respect to variations in ε during practical operation.

4. Conclusions

In summary, we demonstrated, for the first time, that conductivity of PEDOT:PSS as high as 1335 S cm^{-1} could be obtained by

combining the blending and dipping methods with an anionic surfactant, SDS, which were compatible with natural and synthetic fabrics. We also fabricated highly conductive and stretchable fabric heaters using SDS-modified PEDOT:PSS. The mechanisms of conductivity enhancement by SDS dipping and blending methods were elucidated; specifically, the SDS dipping method selectively removed insulating PSS domains, leading to enhancement of the interchain interactions between conducting domains, whereas SDS blending caused conformational change of PEDOT chains. The fabric heaters fabricated using SDS-modified PEDOT:PSS exhibited reversible electrical behaviours with cyclic loading of a tensile strain greater than 80%. The interfibrillar contact effect of the woven fabrics caused a significant but small increase in resistance compared with the calculated value for a rigid substrate. The heat capacity and the convective heat transfer coefficient of BD-PEDOT:PSS-cotton obtained in this work were 2 J K^{-1} and 30 W m^2 K^{-1}, respectively. The effective, simple, and cost-effective method proposed in this work should be useful for fabricating highly conductive PEDOT:PSS-fabric and could expand the use of e-textiles in stretchable applications.

Acknowledgements

This work was supported by a grant from the Institute for Information & Communications Technology Promotion (IITP) funded by the Korean government (MSIP; B0117-16-1003, fundamental technologies of two-dimensional materials and devices for the platform of new-functional smart devices).

References

1 RF Service, Electronic textiles charge ahead, *Science*, 2003, **301**, 909–911.
2 J. Kim, J. Lee, D. Son, M. K. Cho and D. Kim, Deformable devices with integrated functional nanomaterials for wearable electronics, *Nano Convergence*, 2016, **3**, 1–13.
3 T. Q. Trung and N.-E. Lee, Flexible and stretchable physical sensor integrated platforms for wearable human-activity monitoring and personal healthcare, *Adv. Mater.*, 2016, **28**, 4338–4372.
4 M. Amjadi, K.-U. Kyung, I. Park and M. Sitti, Stretchable, skin-mountable, and wearable strain sensors and their potential applications: a review, *Adv. Funct. Mater.*, 2016, **26**, 1678–1698.
5 J.-H. Bahk, H. Fang, K. Yazawa and A. Shakouri, Flexible thermoelectric materials and device optimization for wearable energy harvesting, *J. Mater. Chem. C*, 2015, **3**, 10362–10374.
6 J.-H. Choi, *et al.*, An electroactive, tunable, and frequency selective surface utilizing highly stretchable dielectric elastomer actuators based on functionally antagonistic aperture control, *Small*, 2016, **12**, 1840–1846.
7 C. Larson, *et al.*, Highly stretchable electroluminescent skin for optical signaling and tactile sensing, *Science*, 2016, **351**, 1071.
8 H. R. Mattila, *Intelligent Textiles and Clothing*, Woodhead, Cambridge, U.K., 2006.
9 X. Tao, *Wearable Electronics and Photonics*, Woodhead, Cambridge, U.K., 2003.
10 J. Zhou, *et al.*, High-ampacity conductive polymer microfibers as fast response wearable heaters and electromechanical actuators, *J. Mater. Chem. C*, 2016, **4**, 1238.
11 K. Opwis, D. Knittel and J. S. Gutmann, Oxidative *in situ* deposition of conductive PEDOT:PTSA on textile substrates and their application as textile heating element, *Synth. Met.*, 2012, **162**, 1912–1918.
12 A. Laforgue, Electrically controlled colour-changing textiles using the resistive heating properties of PEDOT nanofibers, *J. Mater. Chem.*, 2010, **20**, 8233–8235.
13 H. K. Park, *et al.*, Flexible plane heater: graphite and carbon nanotube hybrid nanocomposite, *Synth. Met.*, 2015, **203**, 127–134.
14 K.-Y. Shin, J.-Y. Hong, S. Lee and J. Jang, High electrothermal performance of expanded graphite nanoplatelet-based patch heater, *J. Mater. Chem.*, 2012, **22**, 23404.
15 J. J. Bae, *et al.*, Heat dissipation of transparent graphene defoggers, *Adv. Funct. Mater.*, 2012, **22**, 4819–4826.
16 K.-Y. Chun, *et al.*, Highly conductive, printable and stretchable composite films of carbon nanotubes and silver, *Nat. Nanotechnol.*, 2010, **5**, 853–857.
17 J. Yan and Y. G. Jeong, Highly elastic and transparent multiwalled carbon nanotube/polydimethylsiloxane bilayer films as electric heating materials, *Mater. Des.*, 2015, **86**, 72–79.
18 T. J. Kang, T. Kim, S. M. Seo, Y. J. Park and Y. H. Kim, Thickness-dependent thermal resistance of a transparent glass heater with a single-walled carbon nanotube coating, *Carbon*, 2011, **49**, 1087–1093.
19 Y.-H. Yoon, *et al.*, Transparent film heater using sing-walled carbon nanotubes, *Adv. Mater.*, 2007, **19**, 4284–4287.
20 D. S. Hecht, L. Hu and G. Irvin, Emerging transparent electrodes based on thin films of carbon nanotubes, graphene, and metallic nanostructures, *Adv. Mater.*, 2011, **23**, 1482–1513.
21 Y. Ding, M. A. Invernale and G. A. Sotzing, Conductivity trends of PEDOT-PSS impregnated fabric and the effect of conductivity on electrochromic textile, *ACS Appl. Mater. Interfaces*, 2010, **2**, 1588–1593.
22 Y. Wang, Research progress on a novel conductive polymer-poly(3,4-ethylenedioxythiophene) (PEDOT), *J. Phys.: Conf. Ser.*, 2009, **152**, 012023.
23 M. Reyes-Reyes, I. Cruz-Cruz and R. López-Sandoval, Enhancement of the electrical conductivity in PEDOT:PSS films by the addition of dimethyl sulfate, *J. Phys. Chem. C*, 2010, **114**, 20220–20224.
24 Y. Xia, K. Sun and J. Ouyang, Solution-processed metallic conducting polymer films as transparent electrode of optoelectronic devices, *Adv. Mater.*, 2012, **24**, 2436–2440.
25 B. Fan, X. Mei and J. Ouyang, Significant conductivity enhancement of conductive poly(3,4-ethylenedioxythiophene):poly(styrenesulfonate) films by

adding anionic surfactant into polymer solution, *Macromolecules*, 2008, **41**, 5971–5973.

26 N. Kim, *et al.*, Highly conductive PEDOT:PSS nanofibrils induced by solution-processed crystallization, *Adv. Mater.*, 2014, **26**, 2268–2272.

27 D. A. Mengistie, M. A. Ibrahem, P.-C. Wang and C.-W. Chu, Highly conductive PEDOT:PSS treated with formic acid for ITO-free polymer solar cells, *ACS Appl. Mater. Interfaces*, 2014, **6**, 2292–2299.

28 D. Alemu, H.-Y. Wei, K.-C. Ho and C.-W. Chu, Highly conductive PEDOT:PSS electrode by simple treatment with methanol for ITO-free polymer solar cells, *Energy Environ. Sci.*, 2012, **5**, 9662–9671.

29 O. Bubnova and X. Crispin, Towords polymer-based organic thermoelectric generators, *Energy Environ. Sci.*, 2012, **5**, 9345–9362.

30 M. Stavytska-Barba and A. M. Kelley, Surface-enhanced Raman study of the interaction of PEDOT:PSS with plasmonically active nanoparticles, *J. Phys. Chem. C*, 2010, **114**, 6822.

31 S. Sakamoto, M. Okumura, Z. Zhao and Y. Furukawa, Raman spectral changes of PEDOT-PSS in polymer light-emitting diodes upon operation, *Chem. Phys. Lett.*, 2005, **412**, 395–398.

32 Y.-Y. Lee, G. M. Choi, S.-M. Lim, J.-Y. Cho, I.-S. Choi, K. T. Nam and Y.-C. Joo, Growth mechanism of strain dependent morphological change in PEDOT:PSS films, *Sci. Rep.*, 2016, **6**, 25332.

33 Y. Xiao, J.-Y. Lin, S.-Y. Tai, S.-W. Chou, G. Yue and J. Wu, Pulse electropolymerization of high performance PEDOT/MWCNT counter electrodes for PT-free dye-sensitized solar cells, *J. Mater. Chem.*, 2012, **22**, 19919–19925.

34 J. Lee and W. Choi, Surface modification of sulfur cathodes with PEDOT:PSS conducting polymer in lithium–sulfur batteries, *J. Electrochem. Soc.*, 2015, **162**, A935–A939.

35 S. Timpanaro, M. Kemerink, F. J. Touwslager, M. M. De Kok and S. Schrader, Morphology and conductivity of PEDOT/PSS films studied by scanning-tunneling microscopy, *Chem. Phys. Lett.*, 2004, **394**, 339–343.

36 Y.-Y. Lee, *et al.*, Stretching-induced growth of PEDOT-rich cores: a new mechanism for strain-dependent resistivity change in PEDOT:PSS films., *Adv. Funct. Mater.*, 2013, **23**, 4020–4027.

37 D. J. Lipomi, J. A. Lee, M. Vosgueritchian, B. C.-K. Tee, J. A. Bolander and Z. Bao, Electronic properties of transparent conductive films of PEDOT:PSS on stretchable substrates, *Chem. Mater.*, 2012, **24**, 373–382.

38 H. Sun, N. Pan and R. Postle, On the Poisson's ratios of a woven fabric, *Compos. Struct.*, 2005, **68**, 505–510.

39 A. M. Gaikwad, A. M. Zamarayeva, J. Rousseau, H. W. Chu, I. Derin and D. A. Steingart, Highly stretchable alkaline batteries based on an embedded conductive fabric, *Adv. Mater.*, 2012, **24**, 5071.

40 X. Yu, X. Su, K. Yan, H. Hu, M. Peng, X. Cai and D. Zou, Stretchable, conductive, and stable PEDOT-modified textiles through a novel *in situ* polymerization process for stretchable supercapacitors, *Adv. Mater. Technol.*, 2016, 1600009.

41 S. Ji, W. He, K. Wang, Y. Ran and C. Ye, Thermal response of transparent silver nanowire/PEDOT:PSS films heaters, *Small*, 2014, **10**, 4951–4960.

42 O. Laguerre, S. B. Amara, M. C. Charrier-Mojtabi, B. Lartique and D. Flick, Experimental study of air flow by natural convection in a closed cavity: application in a domestic refrigerator, *J. Food Eng.*, 2008, **85**, 547–560.